Isotactic polypropylene/hydrogenated oligocyclopentadiene blends: influence of annealing on crystal and phase structures

E. Martuscelli
Istituto di Ricerche su Tecnologia dei Polimeri e Reologia, C.N.R., Via Toiano 6, 80072 Arco Felice, Napoli, Italy

and M. Canetti, A. M. Bonfatti and A. Seves
Stazione Sperimentale per la Cellulosa, Carta e Fibre Tessili, Piazza Leonardo da Vinci 26, 20133 Milano, Italy
(Received 23 November 1989; revised 8 March 1990; accepted 16 March 1990)

The influence of annealing on phase structure and morphology of isothermally crystallized samples of isotactic polypropylene/hydrogenated oligocyclopentadiene (iPP/HOCP) blends was investigated by using wide- and small-angle X-ray scattering methods and differential scanning calorimetry. The two components are melt-compatible; moreover during crystallization of iPP the molecules of HOCP are mainly ejected in interlamellar regions where they form a homogeneous phase with uncrystallized iPP molecules or part of them. It was found that the presence of such molecules in interlamellar regions determines a loss of thickening tendency of crystalline lamellae following the annealing. The amount of this effect is dependent on composition and undercooling.

(Keywords: isotactic polypropylene; hydrogenated oligocyclopentadiene; blends; annealing; crystal structure; phase structure)

INTRODUCTION

The crystallization and thermal behaviour of blends of isotactic polypropylene (iPP) and hydrogenated oligocyclopentadiene (HOCP) have been studied by Martuscelli *et al.*[1]. It was found that the spherulite growth rate, the overall crystallization rate as well as the equilibrium melting point of iPP were drastically depressed by the addition of HOCP to iPP. From these results the authors concluded that the two components are miscible in the melt. This hypothesis was in agreement with the observation that iPP/HOCP blends showed a single composition-dependent glass transition temperature[1].

Small-angle X-ray scattering studies, performed on isothermally crystallized samples of iPP/HOCP blends, showed that the long period, that is the average distance between the barycentre of two adjacent iPP crystalline lamellae, as well as the amorphous interlamellar thickness, increase with the HOCP content while the lamellar thickness remains almost constant[2].

Such results led to the conclusion that in the solid state, that is below the crystallization temperature of iPP, the molecules of HOCP are mainly located in interlamellar regions where they form, with uncrystallized iPP molecules, a homogeneous amorphous solution[2]. This phase structure causes an improvement of low-strain mechanical tensile properties (modulus and yield stress) as shown by Martuscelli *et al.*[3].

From refs. 1, 2 and 3 it was possible to conclude that HOCP acts as diluent of iPP but at the same time, due to its high T_g and to the particular phase structure realized after crystallization of iPP, it also works as a molecular reinforcing agent.

The present paper deals with a SAXS and WAXS study on the influence of different annealing processes on the phase structure of isothermally crystallized samples of iPP/HOCP blends. The main goal of the work is to elucidate how the presence of molecules of HOCP in interlamellar regions of iPP may influence the thickening mechanism caused by annealing.

EXPERIMENTAL

Materials

Binary blends of isotactic polypropylene (Moplen T30SX, M_w 300 000; Montedison) and hydrogenated oligocyclopentadiene (HOCP) (Escorez, M_w 630; Esso Chemical) were prepared by melt mixing the polymers in a microextruder. The weight mixing ratios of polypropylene/hydrogenated oligocyclopentadiene (iPP/HOCP) were 90/10, 70/30 and 50/50. Blends and plain iPP were melted at 473 K for 10 min, then isothermally crystallized. The crystallization temperatures (T_c) were calculated according to the relation:

$$T_c = T_m^\circ - \Delta T$$

where T_m° are the equilibrium melting temperatures, experimentally obtained in a previous work[1], and ΔT is the undercooling, which was chosen constant for every isothermal crystallization. Then all the isothermally crystallized samples were annealed at the annealing temperature (T_a), calculated according to the relation:

$$T_a = T_c + 17\ \mathrm{K}$$

This work refers to samples of iPP and iPP/HOCP blends isothermally crystallized and annealed for 24 h

0032-3861/91/040641-07

Table 1 Temperature of crystallization (T_c) and temperature of annealing (T_a) of plain iPP and blends

	Isothermally crystallized samples, $\Delta T = 65.4$ K		Isothermally crystallized samples, $\Delta T = 59.3$ K	
iPP/HOCP	T_c (K)	T_a (K)	T_c (K)	T_a (K)
100/0	396.0	413.0	402.1	419.1
90/10	393.7	410.7	399.8	416.1
70/30	389.9	406.9	396.0	413.0
50/50	385.8	402.8	393.9	410.9

according to two different procedures, namely:

procedure number one

$$\Delta T = 65.4 \text{ K} \qquad T_a = T_c + 17 \text{ K}$$

procedure number two

$$\Delta T = 59.3 \text{ K} \qquad T_a = T_c + 17 \text{ K}$$

The details of the crystallization and annealing for each sample are reported in *Table 1*. Isothermally crystallized and annealed samples were analysed by d.s.c., WAXS and SAXS techniques.

Differential scanning calorimetry

The samples were analysed by a Perkin–Elmer DSC-4 Thermal Analysis Data Station (TADS) system. The samples (about 5 mg) were heated from 313 to 573 K at a scanning rate of 10 K min^{-1}. The melting temperature and the apparent enthalpies of fusion were obtained from the maximum and the area of the endothermic peaks.

Wide-angle X-ray scattering

The WAXS data were obtained by a Siemens D-500 diffractometer, with a Siemens FK 60-10, 2000 W Cu tube. The samples were mounted on a specimen carrier for specimen spinning with a rotational speed of 30 rpm. The line-broadening data were collected with a scanning rate of 0.1 deg (2θ)/min. A nickel standard sample was employed to determine the instrumental broadening.

Small-angle X-ray scattering

SAXS data were measured at 25°C, using a Huber 701 chamber with a monochromator glass block[4] and a resolution of about 1100 Å. Monochromatized Cu K_α X-rays (wavelength $\lambda = 1.542$ Å) were supplied by a stabilized Siemens Kristalloflex 710 generator and a Siemens FK 60-04. 1500 W copper target tube. The scattered intensity was measured using a Siemens scintillator counter with NaI(Tl) scintillator crystal and beryllium window. The intensity was counted at each of 80 angles of measurement in the interval from 0.08 to 1.52 deg (2θ). To reduce the statistical error of counting, for each sample, the mean intensity values were obtained from seven scans with a time of 18 h for a complete measurement. The standard deviations calculated for the intensity values at each counting angle showed a low degree of spread of the intensity data around the average values. The camera and the counting equipment were controlled by a Huber SMC 9000 interfaced with an Olivetti M 24 computer. The raw data were first corrected for sample absorption and then the background was subtracted. The collimation error was removed by applying the Glatter method[5] to obtained desmeared scattering data.

RESULTS AND DISCUSSION

Thermal behaviour

The apparent enthalpies of fusion ΔH^* of plain iPP and blends were calculated from the area of the d.s.c. endothermic peaks. The crystalline and amorphous weight fractions were calculated from the following relations:

$$\omega_{cr} = \Delta H^*/\Delta H_{PP} \qquad \omega_{am} = 1 - \omega_{cr} \tag{1}$$

where ΔH_{PP} (44 cal g^{-1}) is the heat of melting per gram of 100% crystalline iPP[6].

The crystalline weight fractions referred to the iPP were calculated from:

$$\omega_{crPP} = \omega_{cr}/X_{PP} \tag{2}$$

where X_{PP} is the weight fraction of iPP in the blends.

As shown by the data reported in *Table 2* the crystallinity of the blends (ω_{cr}) decreases on increasing the HOCP content, while the crystallinity of the iPP component (ω_{crPP}) increases (*Figures 1a* and *1b*). The annealing produced a general enhancement of the crystallinity (*Table 2* and *Figures 1a* and *1b*).

Plots of the observed calorimetric melting temperature (T_m) against HOCP weight fraction for plain iPP and iPP/HOCP blends are shown in *Figure 2*. The melting

Table 2 Melting temperature (T_m), amorphous and crystalline weight fractions (ω_{am}), ω_{cr} and crystallinity of iPP component (ω_{criPP}) of plain iPP and blends

	Isothermally crystallized samples, $\Delta T = 65.4$ K				Annealed samples			
iPP/HOCP	T_m (K)	ω_{am}	ω_{cr}	ω_{crPP}	T_m (K)	ω_{am}	ω_{cr}	ω_{crPP}
100/0	437.1	0.486	0.514	0.514	440.1	0.467	0.533	0.533
90/10	435.5	0.533	0.467	0.519	437.5	0.485	0.515	0.572
70/30	430.6	0.610	0.390	0.557	434.1	0.568	0.432	0.617
50/50	427.5	0.680	0.320	0.640	431.3	0.661	0.339	0.678
	Isothermally crystallized samples, $\Delta T = 59.3$ K				Annealed samples			
iPP/HOCP	T_m (K)	ω_{am}	ω_{cr}	ω_{crPP}	T_m (K)	ω_{am}	ω_{cr}	ω_{crPP}
100/0	439.6	0.482	0.518	0.518	442.1	0.454	0.546	0.546
90/10	436.9	0.502	0.498	0.553	439.4	0.482	0.518	0.576
70/30	432.6	0.577	0.423	0.604	435.1	0.563	0.437	0.624
50/50	428.9	0.652	0.348	0.696	432.1	0.620	0.380	0.760

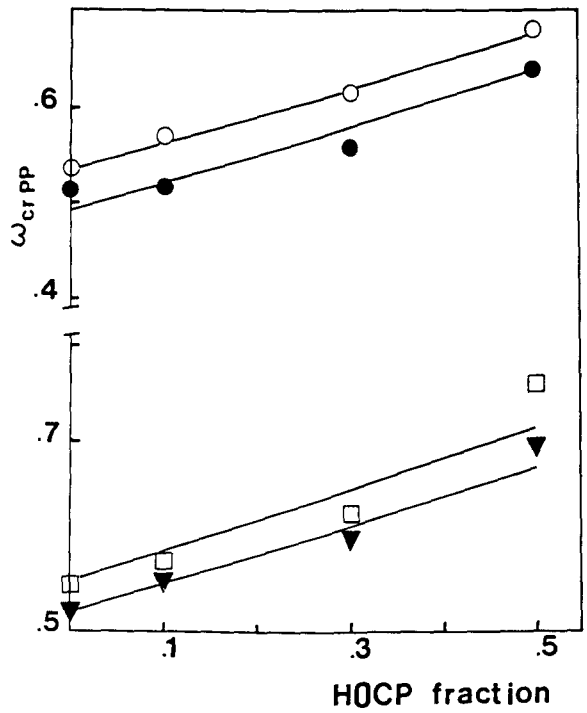

Figure 1 Crystallinity of iPP component *versus* HOCP fraction. Isothermal crystallization at $\Delta T = 65.4$ K (●) and annealing (○). Isothermal crystallization at $\Delta T = 59.3$ K (▼) and annealing (□)

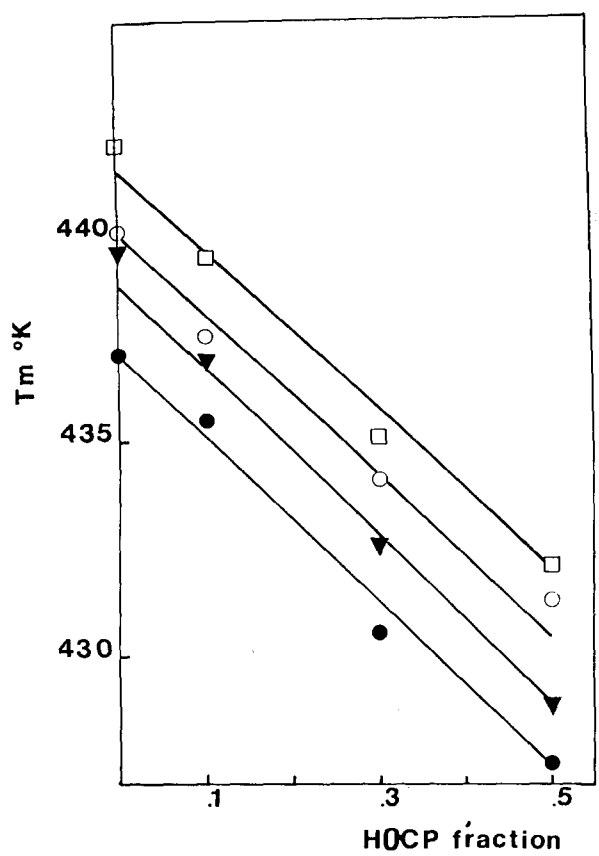

Figure 2 Melting point *versus* HOCP fraction. Isothermal crystallization at $\Delta T = 65.4$ K (●) and annealing (○). Isothermal crystallization at $\Delta T = 59.3$ K (▼) and annealing (□)

temperature decreases linearly with HOCP fraction, according with our previous findings reported in ref. 1, where compatibility in the melt at molecular level of iPP and HOCP was suggested. It can be observed that, for both plain iPP and blends, an increase of melting temperature is produced by annealing (see *Figure 2*).

Wide-angle X-ray scattering studies

WAXS diffractograms of plain iPP and of iPP/HOCP 70/30 blends are shown in *Figure 3*. It can be observed that, following the annealing process, in agreement with d.s.c. results, the intensity of the crystalline peaks increases.

The apparent crystal size D of iPP in perpendicular direction to the (1 1 0) (0 4 0) and (1 3 0) crystallographic planes was calculated by the Sherrer equation[7]:

$$D_{hkl} = \frac{K\lambda}{\beta_0 \cos(\theta_{hkl})} \tag{3}$$

where β_0 is the halfwidth in radians of the reflection corrected for instrumental broadening; λ is the wavelength of the radiation used (1.542 Å); and the shape factor K is set equal to unity and so the size data have to be considered as relative data[7].

The crystal size D of plain iPP is systematically lower than that of blends, even though for blends D does not seem to be influenced by the HOCP content; the annealed samples showed a low increment for all investigated crystallographic planes (*Table 3*).

The presence of (2 2 0) reflection allowed the correction for lattice distortion of $D_{(110)}$. As proposed by Morosoff *et al.*[8], we alternatively considered the possible contribution of microstrain and paracrystallinity. The microstrain contribution increased linearly with the order of reflection (n) and the paracrystallinity contribution with the square of the order. The microstrain and paracrystalline factors (Mf, Pf) were obtained from the following expressions:

$$Mf = \frac{1}{(\delta S^2)_0 D_{(110)}} \qquad Pf = \frac{1}{(\delta S)_0 D_{(110)}} \tag{4}$$

where $(\delta S^2)_0$ and $(\delta S)_0$ are respectively the intercepts of the ΔS^2 and ΔS *versus* n^2 plots, and ΔS was obtained by:

$$\Delta S = (\cos\theta)\beta_0/\lambda \tag{5}$$

As reported in *Table 4*, the correction factors were higher in the case of blends and generally the microstrain contribution was more significant than paracrystallinity. These facts together with the increment of the D values can be explained as a slightly higher growth of the crystals in the blends, with a consequent enhancement of the strains. These observations were confirmed and more obvious after the annealing treatment.

Small-angle X-ray scattering studies

For all SAXS measurements the abscissa variable, Q, was calculated by:

$$Q = 4\pi(\sin\theta)/\lambda \tag{6}$$

After Lorentz correction of the desmeared intensities[9], the long period L, defined as the distance between the centres of two adjacent lamellae, was calculated by:

$$L = 2\pi/Q_m \tag{7}$$

where Q_m is the abscissa value at the maximum of the plot.

The radius of gyration (R) can be assumed as a measure of the spatial extent of a whole particle. It is obtained from the innermost part of the scattering curve using the

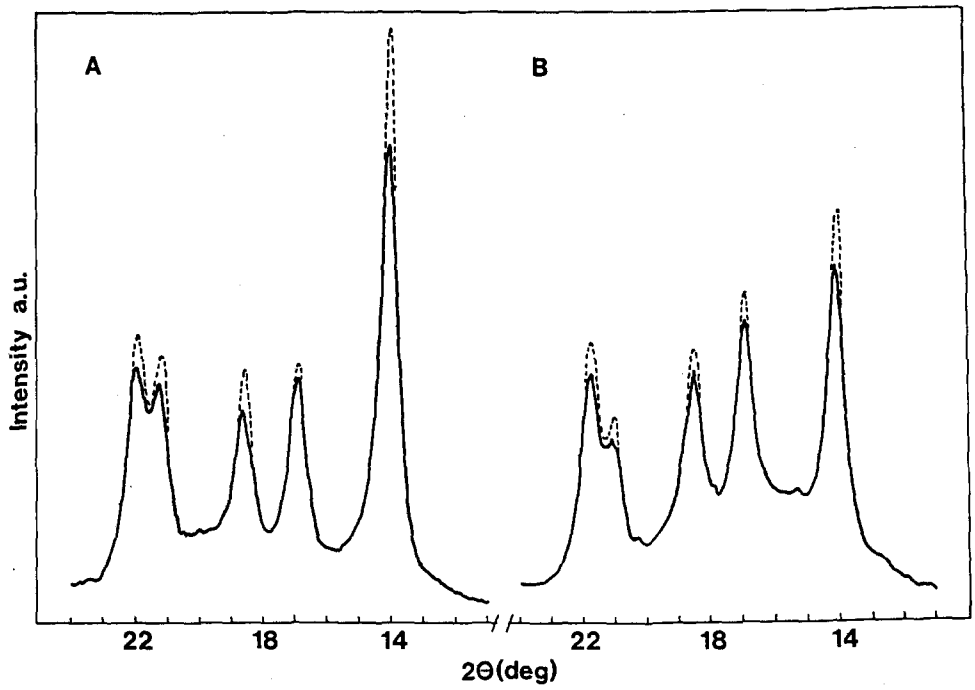

Figure 3 Wide-angle X-ray diffraction. (A) Pure iPP isothermally crystallized at $\Delta T = 59.3$ K (———) and annealed (– – – –). (B) iPP/HOCP 70/30 isothermally crystallized at $\Delta T = 65.4$ K (———) and annealed (– – – –)

Table 3 Apparent crystal size (D) of plain iPP and blends (values in Ångstroms)

	Isothermally crystallized samples, $\Delta T = 65.4$ K			Annealed samples		
iPP/HOCP	(110)	(130)	(040)	(110)	(130)	(040)
100/0	208	210	220	243	238	234
90/10	217	228	236	229	233	263
70/30	210	215	236	227	230	246
50/50	213	231	228	223	221	230
	Isothermally crystallized samples, $\Delta T = 59.3$ K			Annealed samples		
iPP/HOCP	(110)	(130)	(040)	(110)	(130)	(040)
100/0	215	246	211	249	245	225
90/10	225	230	241	227	235	249
70/30	233	238	237	247	248	261
50/50	225	230	241	227	235	245

Table 4 Microstrain and paracrystalline factors (Mf, Pf) of plain iPP and blends

	Isothermally crystallized samples, $\Delta T = 65.4$ K		Annealed samples	
iPP/HOCP	Mf	Pf	Mf	Pf
100/0	1.33	1.17	1.27	1.02
90/10	1.40	1.24	1.90	1.35
70/30	1.50	1.28	1.81	1.34
50/50	1.44	1.24	2.09	1.47
	Isothermally crystallized samples, $\Delta T = 59.3$ K		Annealed samples	
iPP/HOCP	Mf	Pf	Mf	Pf
100/0	1.27	1.18	1.42	1.24
90/10	1.69	1.31	1.76	1.34
70/30	1.75	1.38	2.50	1.40
50/50	1.83	1.34	2.08	1.41

approximation of Guinier and Fournet[10]:

$$I(Q) = I_0 \exp(-Q^2R^2/3) \quad (8)$$

where I_0 and $I(Q)$ are the intensities at angle zero and angle Q, respectively. From the slope ($\tan \alpha$) of the Guinier plot $\ln I(Q)$ *versus* Q^2, the radius of gyration can be obtained as:

$$R = (-3 \tan \alpha)^{1/2} \quad (9)$$

Considering the elongated shape of particles, the radius of gyration of the cross-section (R_c) can be calculated by applying the approximation of Guinier and Fournet[10]:

$$I(Q) = [I(Q)Q]_0 \exp(-Q^2R_c^2/2) \quad (10)$$

where $[I(Q)Q]_0$ is the product $I(Q)Q$ at zero angle. From the slope ($\tan \alpha$) of the plot of $\ln[I(Q)Q]$ *versus* Q^2, the

radius of the cross-section was calculated as:

$$R_c = (-2 \tan \alpha)^{1/2} \quad (11)$$

Likewise, for lamellar particles[11], from the Guinier approximation the radius of gyration of the thickness (R_t) can be calculated by applying:

$$I(Q) = [I(Q)Q^2]_0 \exp(-Q^2R_t^2) \quad (12)$$

where $[I(Q)Q^2]_0$ is the product $I(Q)Q^2$ at zero angle. From the slope (tan α) of $\ln[I(Q)Q^2]$ *versus* Q^2 plots, the R_t value can be obtained as:

$$R_t = (-1 \tan \alpha)^{1/2} \quad (13)$$

The straight lines used for the extrapolations of the radii of gyration showed good correlation coefficients. The radii of gyration values are summarized in *Table 5*.

The lamellar thickness (t) can be calculated from the radius of gyration of the thickness by:

$$t = R_t(12)^{1/2} \quad (14)$$

According to Kratky[12], by the approximation of the particle to a parallelepiped, the lamellar length (l_R) and width (b_R) can be obtained from the three radii of gyration (R, R_c, R_t) by:

$$l_R^2 = 12(R^2 - R_c^2) \qquad b_R^2 = 12(R_c^2 - R_t^2) \quad (15)$$

Table 5 Radius of gyration of the whole particle (R), cross section (R_c) and thickness (R_t) of plain iPP and blends (values in Ångstroms)

	Isothermally crystallized samples, $\Delta T = 65.4$ K			Annealed samples		
iPP/HOCP	R	R_c	R_t	R	R_c	R_t
100/0	59.5	42.5	27.1	74.8	55.8	35.0
90/10	53.3	37.1	24.8	62.5	45.3	27.4
70/30	89.7	59.9	30.1	95.1	62.3	30.8
50/50	94.6	63.3	30.2	99.0	67.1	39.8
	Isothermally crystallized samples, $\Delta T = 59.3$ K			Annealed samples		
iPP/HOCP	R	R_c	R_t	R	R_c	R_t
100/0	59.8	43.6	26.0	79.7	58.5	36.4
90/10	49.9	40.8	22.3	62.1	51.3	30.4
70/30	86.1	58.7	32.1	96.6	67.0	38.3
50/50	91.0	59.9	32.1	108.1	75.2	41.9

The thickness of amorphous interlamellar region (l_a) was calculated by:

$$l_a = L - t \quad (16)$$

The lamellar thickness and long-period values are reported in *Table 6*.

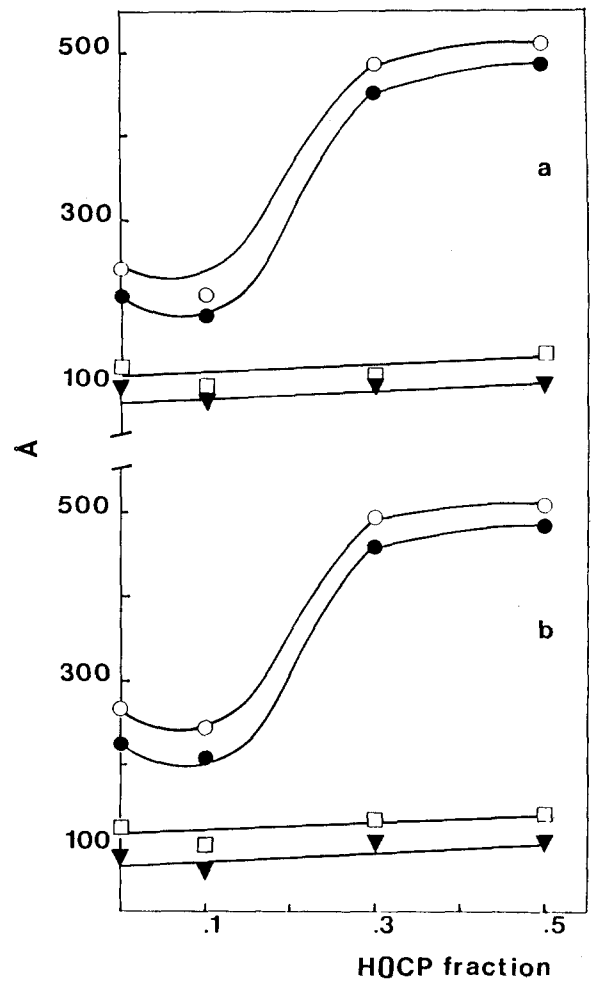

Figure 4 Plots of long periods and lamellar thickness *versus* HOCP fraction. (a) Long period of isothermal crystallization at $\Delta T = 65.4$ K (●) and annealing (○). Lamellar thickness of isothermal crystallization at $\Delta T = 65.4$ K (▼) and annealing (□). (b) Long period of isothermal crystallization at $\Delta T = 59.3$ K (●) and annealing (○). Lamellar thickness of isothermal crystallization at $\Delta T = 59.3$ K (▼) and annealing (□)

Table 6 Long period, lamellar thickness and amorphous interlamellar thickness of plain iPP and blends (Å)

	Isothermally crystallized samples, $\Delta T = 65.4$ K					Annealed samples				
iPP/HOCP	L	l_R	b_R	t	l_a	L	l_R	b_R	t	l_a
100/0	205 ± 10	144	113	94	111	239 ± 13	173	150	121	118
90/10	183 ± 8	133	96	86	97	210 ± 10	149	125	95	115
70/30	450 ± 35	231	179	104	346	483 ± 21	249	188	107	376
50/50	483 ± 21	244	193	105	378	505 ± 23	252	187	138	367
	Isothermally crystallized samples, $\Delta T = 59.3$ K					Annealed samples				
iPP/HOCP	L	l_R	b_R	t	l_a	L	l_R	b_R	t	l_a
100/0	227 ± 9	142	121	90	137	270 ± 13	188	159	126	144
90/10	212 ± 8	100	118	77	135	247 ± 11	121	143	105	142
70/30	460 ± 19	218	170	111	349	493 ± 21	241	191	133	366
50/50	483 ± 21	237	175	111	372	505 ± 23	269	216	145	360

From the data of *Table 6* and the trends of plots of *Figures 4a* and *4b* it emerges that the long spacing of iPP is slightly larger than that of iPP/HOCP (90/10) blends. On the contrary 70/30 and 50/50 blends are characterized by values of L significantly larger than that of plain iPP; moreover the lamellar thickness is almost independent of blend composition. Such a result in addition to the trend of the thickness of the amorphous interlamellar region (*Figures 5a* and *5b*) suggests that the uncrystallizable component is located in the interlamellar regions especially in the case of blends with high HOCP content. The constant trend observed for the lamellar thickness t is accounted for by considering that the crystallization is performed at ΔT constant.

The annealing produced a general increasing of long period (L) and lamellar dimensions (l_R, b_R, t) for pure iPP and blends.

Plotting the melting temperature (T_m), obtained by d.s.c. *versus* the inverse of the lamellar thickness ($1/t$), a straight line was observed. Thus with a certain accuracy the trend of T_m against $1/t$ can be described by the following relation[13]:

$$T_m = T_m^\circ - \frac{2\sigma_e T_m^\circ}{\Delta H_f}\frac{1}{t} \qquad (17)$$

From the intercept the equilibrium melting temperature (T_m°) was deduced (*Figure 6*). The extrapolated T_m° values (*Table 7*) are in quite good agreement with those obtained from the T_m *versus* T_c plots[1] for plain iPP, 90/10 and 70/30 iPP/HOCP blends and lower for the 50/50 blend.

The percentage of long-spacing increment (L_i) of each sample after annealing was calculated by using the following relation:

$$L_i = \frac{L(T_a) - L(T_c)}{L(T_c)} \times 100 \qquad (18)$$

where $L(T_c)$ is the long spacing of the sample isothermally crystallized at T_c and $L(T_a)$ is the long spacing after annealing. As can be seen in *Figure 7*, L_i decreases with the increase of HOCP content. It can be concluded that the process of long-spacing thickening, following an annealing process, is drastically hindered by the presence of HOCP molecules dispersed in interlamellar regions.

The percentage of lamellar thickness increment (t_i) of samples, following annealing, calculated as:

$$t_i = \frac{t(T_a) - t(T_c)}{t(T_c)} \times 100 \qquad (19)$$

is plotted against HOCP content in *Figure 8*. From this it emerges that t_i decreases sharply following annealing in the case of iPP/HOCP blends. Such an effect seems to be dependent upon thermal history. As matter of fact it can be noted that the samples that have undergone treatment 1 show, at least for concentration of HOCP $\leqslant$ 30%, values of t_i considerably larger than those of treatment 2 even though lower than that of neat iPP.

Thus it emerges that the process drastically influenced during annealing of iPP/HOCP samples, isothermally crystallized at relatively low undercooling, is mainly that of crystalline lamellar thickening.

Work is in progress in our institutes to assess the general validity of the conclusions reached by the present paper.

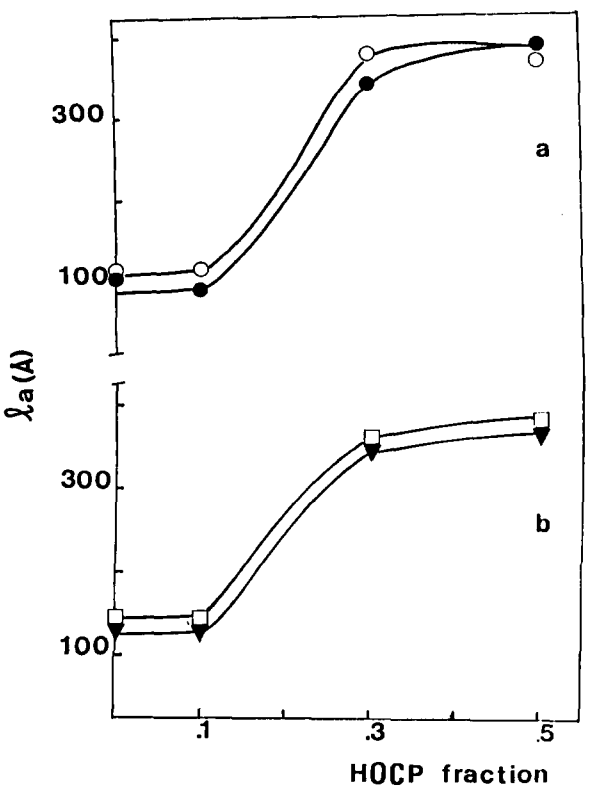

Figure 5 Plots of amorphous interlamellar region *versus* HOCP fraction. (a) Isothermal crystallization at $\Delta T = 65.4$ K (●) and annealing (○). (b) Isothermal crystallization at $\Delta T = 59.3$ K (▼) and annealing (□)

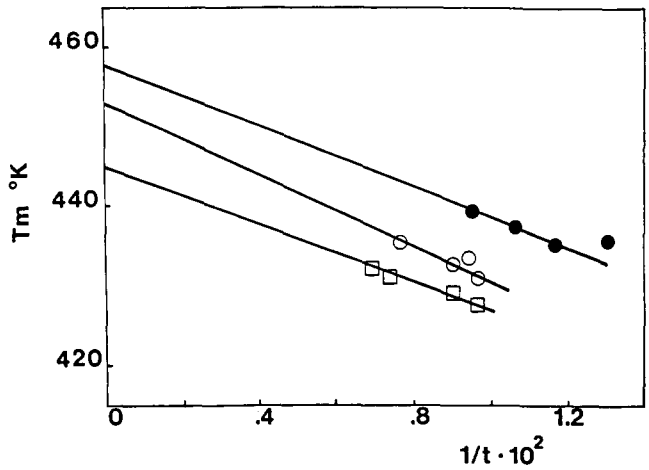

Figure 6 Plots of melting temperature (T_m) *versus* the inverse of lamellar thickness for iPP/HOCP blends: (●) 90/10; (○) 70/30; (□) 50/50

Table 7 Equilibrium melting temperatures (T_m°) of plain iPP and blends

	T_m°	
iPP/HOCP	From T_m *versus* $1/t$ plots[a]	From T_m *versus* T_c plots[b]
100/0	460	461
90/10	458	459
70/30	453	455
50/50	445	451

[a] Present paper
[b] From ref. 2

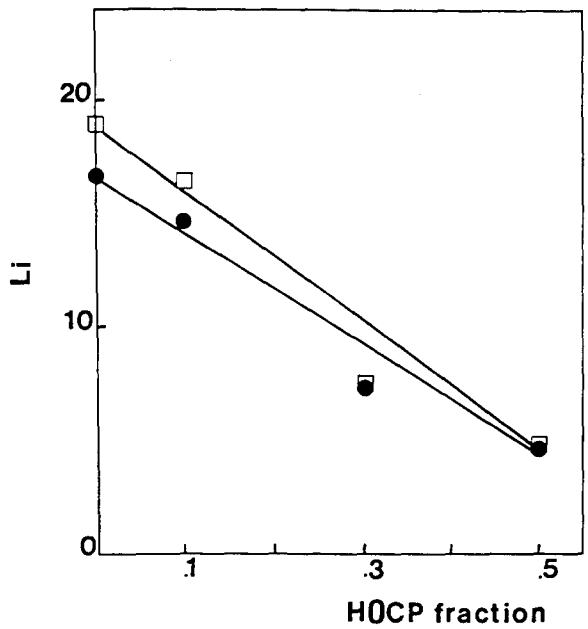

Figure 7 Plots of the percentage of the long-period increment (L_i) *versus* HOCP fraction: (●) isothermally crystallized samples at $\Delta T = 59.3$ K; (□) isothermally crystallized samples at $\Delta T = 65.4$ K

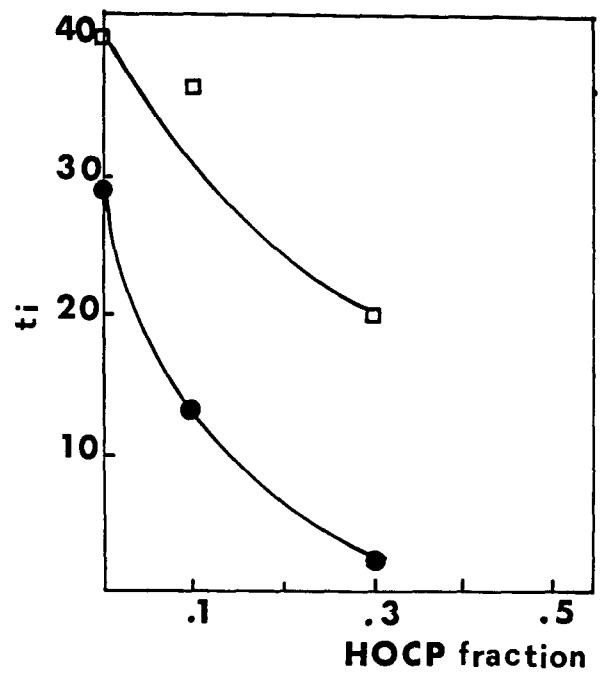

Figure 8 Plots of the percentage of crystalline lamellar thickness increment (t_i), following annealing *versus* HOCP fraction: (●) isothermally crystallized samples at $\Delta T = 59.3$ K; (□) isothermally crystallized samples at $\Delta T = 65.4$ K

REFERENCES

1 Martuscelli, E., Silvestre, C., Canetti, M., De Lalla, C., Bonfatti, A. and Seves, A. *Makromol. Chem.* 1989, **190**, 2615
2 Martuscelli, E., Canetti, M. and Seves, A. *Polymer* 1989, **30**, 304
3 Di Liello, V., Martuscelli, E., Ragosta, G. and Buzio, P. *J. Mater. Sci.* 1989, **24**, 3235
4 Schnabel, E., Hosemann, R. and Rode, B. *J. Appl. Phys.* 1972, **43**, 3237
5 Glatter, O. *J. Appl. Crystallogr.* 1974, **17**, 147
6 Van Krevelen, D. W. 'Properties of Polymers', Elsevier, Amsterdam, 1976
7 Alexander, L. E. 'X-ray Diffraction Method in Polymer Science', Wiley-Interscience, New York, 1969
8 Morosoff, N., Sakaoku, K. and Peterlin, A. *J. Polym. Sci. (A-2)* 1972, **10**, 1221
9 Vonk, C. G. *J. Appl. Crystallogr.* 1973, **6**, 81
10 Guinier, A. and Fournet, G. 'Small Angle Scattering of X-Rays', Wiley-Interscience, New York, 1955
11 Kratky, O. and Porod, G. *Acta Phys. Austriaca* 1948, **2**, 133
12 Kratky, O. and Miholic, G. *J. Polym. Sci. (C)* 1963, **2**, 449
13 Hoffman, J. D. *Polymer* 1982, **24**, 3